

Flexible Wearable Capacitive Sensors Based on Ionic Gel with Full-Pressure Ranges

Mengqin Zhang, Mingxin Gu, Li Shao, Guanyin Cheng, Hailin Gao, Bihao Sun, Sen Li, Tian Tang, Nan Li, Yuanbang Yi, Dacheng Wei, Ce Yang, and Dapeng Wei*



Cite This: *ACS Appl. Mater. Interfaces* 2023, 15, 15884–15892



Read Online

ACCESS |

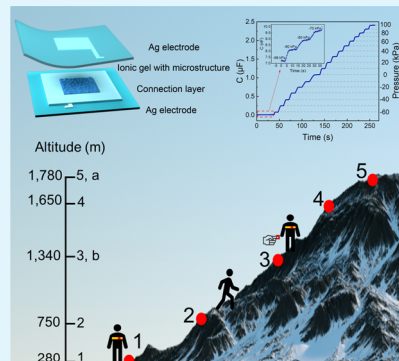
Metrics & More

Article Recommendations

Supporting Information

ABSTRACT: Flexible positive pressure sensors have been studied extensively and have been used in a lot of scenarios. However, negative pressure detection is also in demand in some scenarios, such as fluid mechanics analysis, air pressure sensing, and so on. Flexible wearable sensors that can detect both positive and negative pressures will greatly broaden the application field. In this paper, we report a flexible highly sensitive ionic gel (IG) pressure sensor, which is simple and of low cost to prepare and can reliably detect a large pressure range from -98 to 100 kPa under an atmospheric pressure of about 982 hPa. The IG dielectric layer is composed of polyvinyl alcohol and phosphoric acid with a random microstructure of sandpaper inversion. The sensor exhibits flexibility, cycling stability, and high sensitivity under both negative and positive pressures ($S = 84.45$ nF/kPa for the negative pressure section, $S = 25.61$ nF/kPa for the positive pressure section). These sensors could be worn on the body not only to test breathing and pulse but also to measure air pressure for estimating the altitude, showing that the flexible full-pressure sensors have a wider application range in wearable electronics.

KEYWORDS: ionic gel, negative pressure, flexible electronics, random microstructures, wearable sensors



1. INTRODUCTION

With extensive research on flexible pressure sensors, potential applications in many fields are gradually being developed, such as real-time monitoring of human health,^{1–3} wearable devices,^{4,5} human–computer interaction,^{6,7} and so on. The signal conversion mechanisms of pressure sensors are usually capacitive, resistive, piezoelectric, and frictional.^{8–11} These sensors have their own advantages and disadvantages, but most of them will delaminate and not work under negative pressure. Among them, piezo-capacitive pressure sensors are of great interest due to the advantages of simple structure, low power consumption, and good operating stability.^{12–14} The parallel plate capacitive pressure sensor consists of a dielectric layer sandwiched between two electrodes. Owing to the change of thickness or effective area of the dielectric layer, the capacitance changes under external forces. Theoretically, this structure is capable of measuring both positive and negative pressures. The reason is that the distance between electrodes decreases when positive pressure is applied and increases when negative pressure is applied, thus changing the capacitance. Nevertheless, due to the limited relative variation of the thickness or area of the dielectric layer, the device suffers from low sensitivity and a narrow response range.

These deficiencies have prompted the exploration of methods to increase the range of capacitance variation and improve sensor performance. The use of dielectrics with compressible microstructures has proven to be one of the most

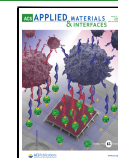
effective methods. Recently, microstructured surfaces that have been widely used are micropyramids,^{15,16} microspheres,^{17,18} microcolumn arrays,^{19,20} and natural templates, such as conical patterns made of plant leaves,^{17,21} among others. In addition, microstructures on electrodes, composite dielectrics, and engineered holes within the dielectric layer can also improve the performance of capacitive pressure sensors.²² However, to detect both positive and negative pressures, many other conditions need to be met. For example, a larger initial capacitance is needed under no pressure, in order to respond through the reduction of capacitance when subjected to a negative pressure, and so forth.

In particular, with advantages, such as high interfacial capacitance, the emerging ionic liquid electrolytes have attracted increasing attention. It has been applied in supercapacitors,^{23–25} lithium-ion batteries,^{26,27} field-effect transistors,^{28,29} and so forth. Meanwhile, ionic liquids are combined with polymer composites to form ionic gels as dielectric layers, which are widely used in pressure sensors and also achieve better sensing performance.^{30–33} The IG has outstanding

Received: January 19, 2023

Accepted: March 1, 2023

Published: March 17, 2023



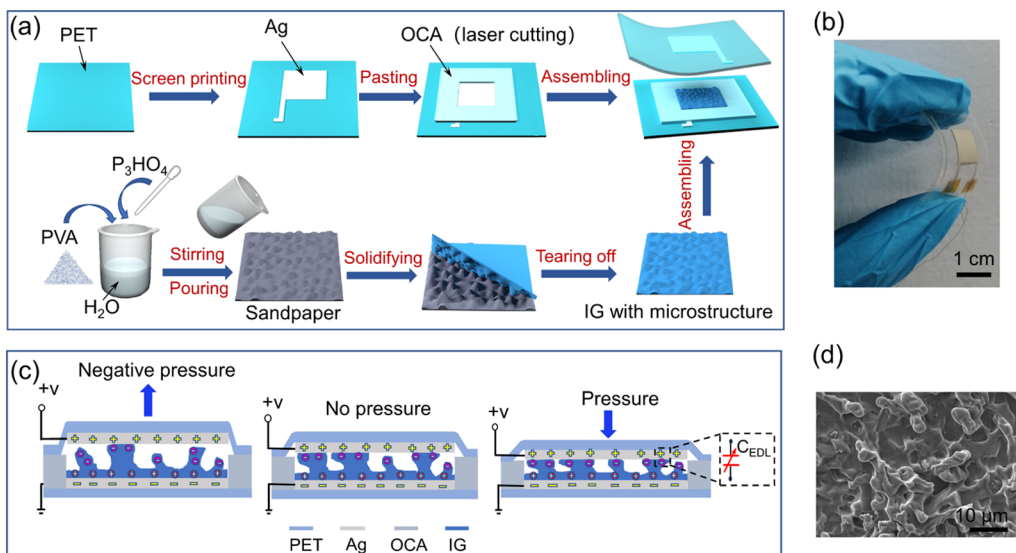


Figure 1. Preparation, mechanism, and characterization of the flexible sensor. (a) Schematic diagram of the preparation process of a flexible capacitive sensor that can detect both positive and negative pressures. (b) Photograph of the sensor with a scale bar of 1 cm. (c) Schematic diagram of the working principle of the sensor. (d) SEM image of an IG with random microstructures obtained by sandpaper with a mesh number of no. 2000#, and a scale bar of 10 μ m.

properties, such as high ionic conductivity, low interfacial resistance, good mechanical strength, and flexibility. On the other hand, the improvement from the expensive and complex photolithography process to the simple and low-cost natural template method leads to easier access to microstructures. Due to the combined effect of the microstructured surface and the interfacial capacitance generated by the electric double layer (EDL) effect of IG, the performance of capacitive pressure sensors has been greatly improved.^{21,31–33} In terms of applications, the vast majority of devices are aimed at a signal feedback of positive pressures such as human activity. There are also scenarios where negative pressure needs to be detected, such as studies on adsorbed organisms,³⁴ pressure distribution in aircraft wings,^{35,36} and so forth. In fact, negative pressure-related sensors have been much less studied. Most pressure sensor devices tend to delaminate and fail to detect negative pressure. The layers of the sensor need to be well bonded to each other. Among few existing positive and negative pressure flexible detectors,^{35–38} all of them measure the negative pressure by changing the distance between the two parallel pole plates of the capacitor. And the preparation process is complicated and the test range is small. Therefore, it is necessary to study the simple preparation of negative pressure flexible sensors with a larger pressure range.

Here, we report a capacitive flexible pressure sensor that can measure both positive and negative pressure. It is simple to prepare and the layers are firmly bonded. The test range of positive and negative pressure is from −98 to 100 kPa, when atmospheric pressure is about 982 hPa. The IG film with a random microstructure obtained by curing on sandpaper is used as a dielectric layer. The sensor is vacuum laminated and encapsulated under a certain pre-pressure. The resulting EDLs formed at the contact interface generate a large capacitance for testing negative pressure. The upper and lower electrodes are bonded with optically clear adhesive (OCA) around the contact with the IG film to form a hermetic state. This allows the microstructured film to increase or decrease the contact area of the EDL under both positive and negative pressure.

And then the corresponding change in capacitance is obtained. Besides, due to the strong bonding of the OCA to the polyethylene terephthalate (PET) after pre-pressure lamination, the sensor does not delaminate under a pressure of −98 kPa.

2. RESULTS AND DISCUSSION

2.1. Design of the Flexible Sensor. Figure 1a shows the structure and fabrication process of the sensor. The flexible ion-capacitance pressure sensor consists of two identical Ag electrodes, an OCA connecting layer, and a microstructured IG film. First, the electrodes are screen-printed with silver paste on a PET substrate with a sensing area of $1 \times 1 \text{ cm}^2$, allowing for low-cost large-area preparation (Figure S1, Supporting Information). Next, IG is obtained using a mixture of polyvinyl alcohol (PVA) and phosphoric acid in different ratios as structural polymers. In addition, the microstructure of the IG surface was obtained by curing on sandpaper with different roughnesses. The detailed process is that a certain amount of IG is poured onto sandpaper with a fixed mold and is peeled off after curing to form a thin film of IG with random microstructures. The thickness of about three to four hundred microns is appropriate. Furthermore, the sensitivity of the films with different thicknesses under negative pressure is compared in Figure S2 (Supporting Information). The film is used as an active dielectric layer that can be transferred to the electrode sensing area with tweezers. Then, the connecting layer is prepared by a laser cutting process, which involves cutting the OCA into a frame structure with a $1.1 \text{ cm} \times 1.1 \text{ cm}$ square in the middle and an overall size of $2 \text{ cm} \times 2 \text{ cm}$. Finally, the two sides of the electrode and the IG dielectric layer are laminated to assemble the device, where the IG is placed in the central region of the connecting layer in contact with the electrode. The photograph of the device is shown in Figure 1b. It is flexible and can be fitted onto the human body. A pre-pressure needs to be given by the laminating process so that the IG film has some contact with the electrode, such that negative pressure can also be tested. Hence, the initial capacitance

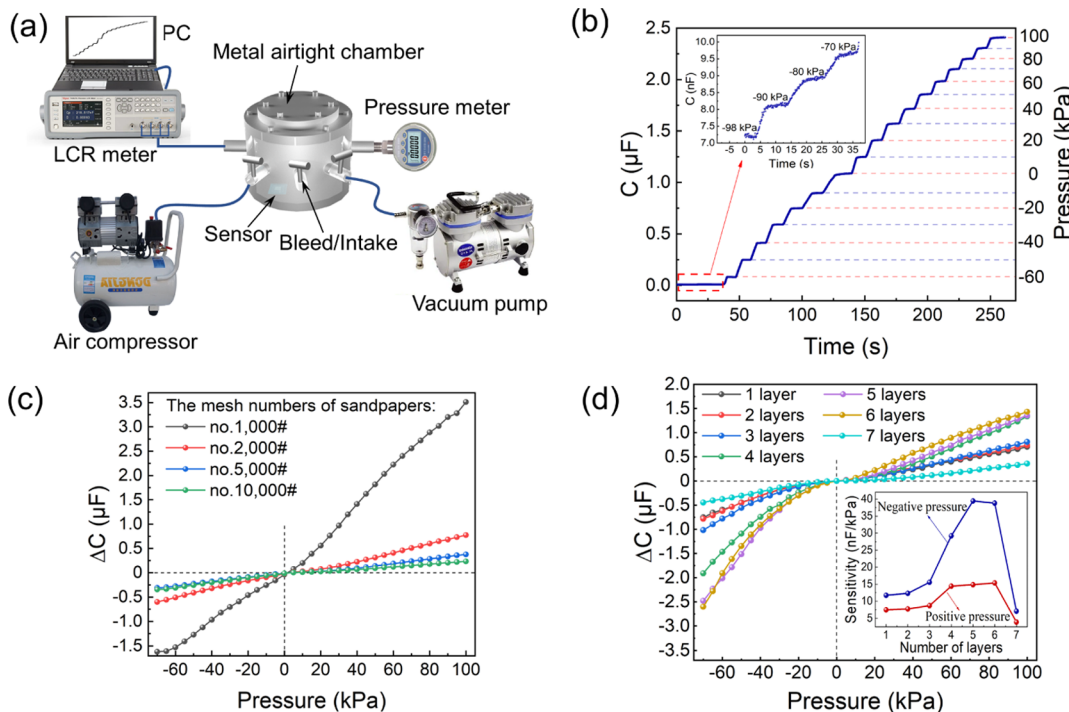


Figure 2. Testing equipment and device's performance variation patterns. (a) Schematic diagram of the equipment for testing device performance in both positive and negative pressure environments. (b) Capacitance variation from -98 to 100 kPa, when atmospheric pressure is about 982 hPa. (c) Pressure sensing performances from IGs with different roughness, which are prepared by sandpapers of different mesh numbers. (d) Pressure sensing performances from different numbers of layers of OCA.

should be larger, and the capacitance can only have a range of decrease in the negative pressure environment. At the same time, a certain compression space has to be reserved to test the positive pressure, and its working principle is shown in Figure 1c. The sensor can detect both the relative state of air pressure and human physiological signals, which has a good prospect in flexible wearable devices, health detection, and so forth.

The protruding portions of the random microstructures were molded from sandpaper depressions, while the grooves and nibbled edges were molded from raised particles. Meanwhile, quantitative information on the surface morphology of the sandpaper template film was investigated by scanning electron microscopy images. It can be seen that the film surface obtained a microstructure opposite to the sandpaper template, in the form of a hemispherical dome, which is irregular and randomly distributed, as shown in Figure 1d. On the other hand, the IG films are opaque due to the light scattering caused by the microstructures. Compared with conventional microfabrication methods, this template process has the advantages of environmental friendliness, simplicity, speed, and low processing cost. The surface structure of the man-made material can be replicated well. It is the abrasive sandpaper that makes the structure more deformable during compression or expansion, extending the range of sensors. Equally important, OCA has a good adhesion on PET, connecting the layers of the device tightly. It also makes a better confined cavity in the middle sensing area and creates conditions for simultaneous detection of positive and negative pressures.

2.2. Working Mechanism of the Flexible Sensor. The microstructures and electrical properties of IG play a crucial role in the performance of the sensor. As shown in Figure 1c, a large number of low molar positive and negative charge ion

pairs are distributed in the IG film. When a voltage is applied, electrons on the electrodes and counter ions in the IG accumulate in a contact region at nanometer distances.^{39,40} Their aggregation increases or decreases when a positive or negative pressure is applied, leading to an increase or decrease in capacitance. The sensing mechanism of the sensor depends on the change of the interfacial capacitance. The Ag electrode and the IG film form the EDLs between the upper and lower contact interfaces. Its capacitance is proportional to the size of the contact area and the ion concentration at a given temperature.⁴¹

The microstructure contributes to the elastic deformation of the membrane under external pressure, which leads to the increase or decrease of the EDL interfacial capacitance. Figure 1c shows a schematic cross-section of the sensor before and after the application of positive and negative pressures. In the initial pre-pressure state, fewer microstructure protrusions are in contact with the electrodes. When positive pressure is applied, not only does the contact area of the existing contact points increase but the lower protrusions also make contact with the electrodes to generate new contact points. Therefore, the effective area of EDL also increases, leading to an increase in capacitance. Conversely, when loaded with negative pressure, the contact between the microstructure and the electrode is reduced and the capacitance decreases. IG films without microstructures, on the other hand, have no corresponding change in capacitance at the same positive or negative pressure, as there is no change in the area of the contact sites. The other side of the film is smooth and the interfacial capacitance remains almost constant. Hence, this irregular microstructure plays an important role in improving the sensitivity and detectable pressure range. According to the Gouy-Chapman-Stern model, such interfaces without electro-

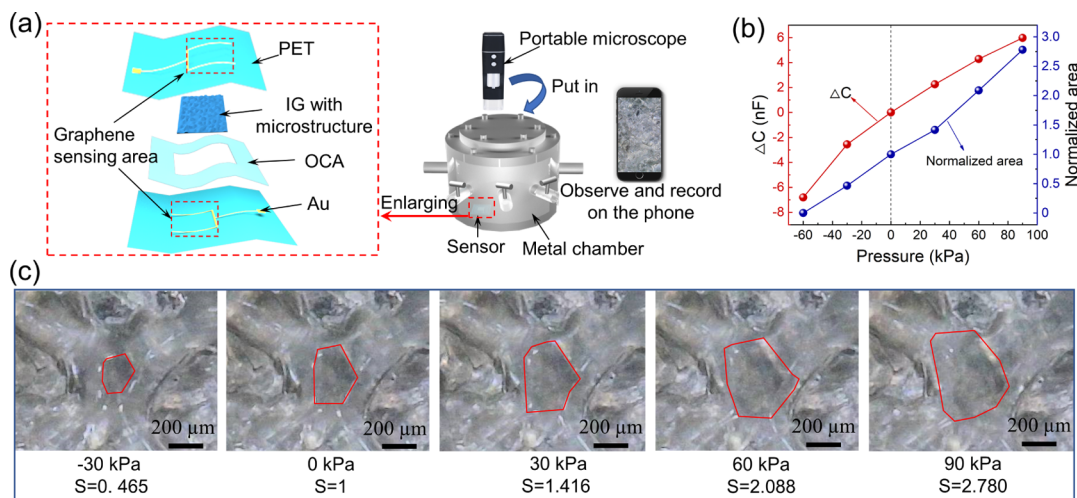


Figure 3. Sensor with transparent electrodes, dynamic observation under a microscope. (a) Schematic diagram of the sensor structure and equipment for microscopical observation. The sensing area of the device is $5\text{ mm} \times 5\text{ mm}$ with transparent graphene electrodes. (b) Air pressure is proportional to the change of sensor capacitance. (c) Microscopic images of IG with a mesh number of no. 100# at different air pressures. The change in the area of the contact point is marked.

chemical reactions can be simply modeled as capacitive elements.⁴²

2.3. Testing Process and Law Analysis. The test equipment and method are shown in Figure 2a. The sensor is placed flat and secured to the bottom of an airtight metal chamber. The sensor electrode leads are connected to the interface inside the chamber, while the LCR tester is connected to the outside to record the capacitance change. An air compression pump and a vacuum pump are connected to the two ports of the chamber to provide either a positive or a negative pressure environment. The air inlet or extraction rate is controlled by a valve, the air pressure in the chamber is read in real time by a digital pressure gauge and the air tightness meets the test requirements in a short time. Our tests were all performed at pressures ranging from -98 to 100 kPa , but the sensors did not reach saturation. For safety reasons, the positive pressure is only given up to a maximum of 100 kPa , and the actual measurable range may be larger. To start with, the air pressure is pumped down to -98 kPa , which is close to an absolute pressure of 0 kPa , because the atmosphere pressure is about 982 hPa when testing. Then, the air is fed in a gradient of 10 kPa and held for a few seconds until it rises back to atmospheric pressure. Lastly, the vacuum pump is turned off and the air compressor is turned on at the same time. Similarly, every 10 kPa rise is held for a few seconds. The corresponding capacitance change is measured, as shown in Figure 2b. Because the testing time cannot be set automatically, the time difference during the test can be ignored and does not affect the test results. It is clear that the change of capacitance is positively correlated with air pressure in a stepwise manner.

The relationship between different grit sizes of sandpaper on sensor performance is explored in Figure 2c, with the different grit sizes representing microstructures of different heights and sizes. We used sandpaper with a mesh number between no. 1000# and no. 10,000#, as performances below no. 1000# are too poor. The results suggest that the smaller the mesh number is, the better the sensor performance is, as shown by the higher sensitivity. The sensor relies on the change of contact between the microstructure and the electrode. The larger mesh number means the smaller roughness and microstructure, which makes electrode contact changes more limited in the test process.

Inversely, coarser microstructure bumps allow for a greater range of variation. But when roughness goes beyond a certain range, its contact points would be too few, leading to degradation of performance. Therefore, there has to be a balance between the roughness of the IG microstructure and the number of contact points in order to guarantee the performance of the sensor, and no. 1000# is the turning point. In addition, the effects of phosphoric acid content and the ratio of PVA to water on the performance of the prepared sensors were also explored (Figures S3 and S4, Supporting Information). Within a certain range, the phosphoric acid content is proportional to the sensor sensitivity, and there is also a turning point beyond which the sensitivity decreases.

The effect of different thicknesses of the OCA connecting layer on the performance of the sensor is shown in Figure 2d. When the thickness of the IG is constant, the change in the thickness of OCA leads to a change in the contact between the IG and electrode, which affects the performance of the sensor. The sensors were prepared using IG film with a thickness of $392\text{ }\mu\text{m}$ and OCA films from 1 to 7 layers. The thickness of one layer of OCA is $100\text{ }\mu\text{m}$. It is noted that the sensitivity of the sensor increases sequentially with six layers. But the sensitivity suddenly goes down when adding up to seven layers. The reason is probably that the PET substrate has a certain hardness and the contact between IG and electrodes is limited when the thickness of IG is higher than the surrounding connecting layer. This phenomenon is gradually alleviated as the surrounding thickness gets closer to the IG. And when the surrounding thickness is larger than the IG, the vacuum extracts the air and fits the upper electrode closely to the IG, which makes the sensitivity of the sensor increase. But after the surrounding thickness exceeds a certain range, the contact between IG and electrodes is reduced and the performance decreases. This is visualized in the initial capacitance of sensors, which gradually increases from the first to the sixth layers and then decreases rapidly.

The sensing interface under different air pressures was observed to verify the working principle of the sensor. The transparent graphene electrodes were used instead of Ag electrodes. The sensor structure and observation process are shown in Figure 3a. The sensing area is $5\text{ mm} \times 5\text{ mm}$, and the

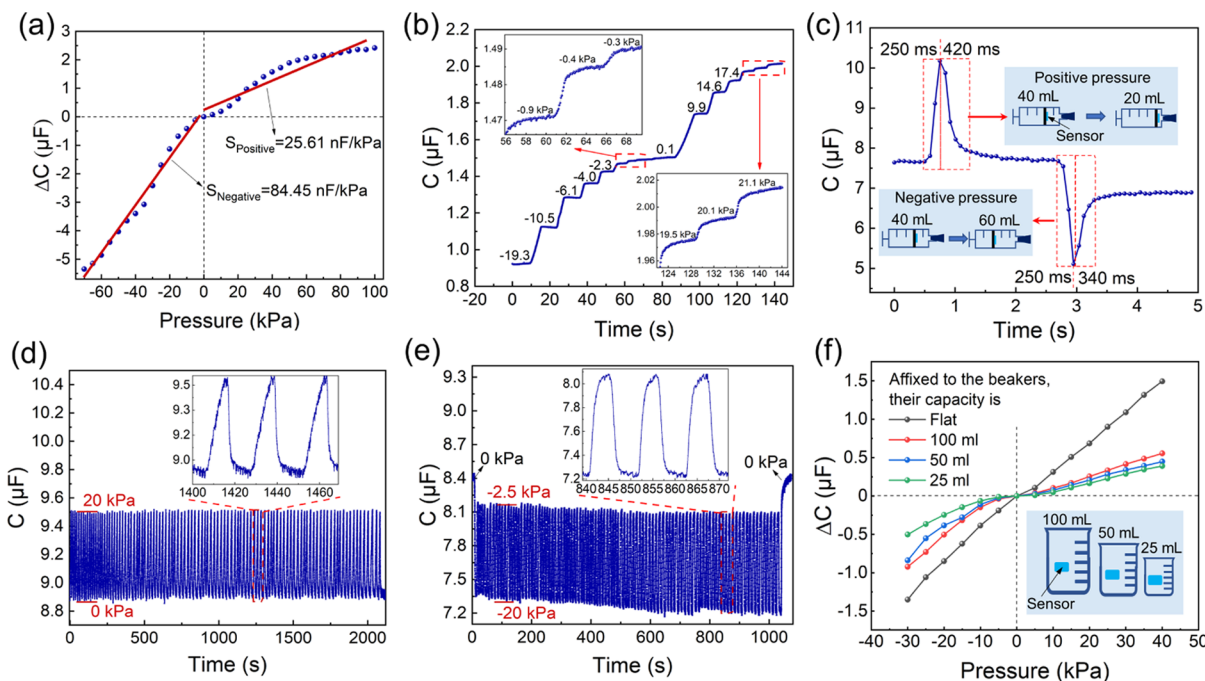


Figure 4. Performance testing of the flexible sensor. (a) Capacitance change (ΔC) as a function of positive and negative pressure. (b) Sensor has a positive pressure detection limit of 1 kPa and a negative pressure detection limit of 0.1 kPa. (c) Response time test using a syringe. (d) Positive pressure cycling test. (e) Negative pressure cycling test. (f) Comparison of the sensor with different bending curvatures.

Table 1. Comparison of Our Flexible Sensor with Other Related Reports

sensing mechanism	dielectric material	sensitivity	pressure range of testing	references
Capacitive	air gap	0.0012–0.0077 kPa ⁻¹	−60–20 kPa	37
Capacitive	air gap	0.28 kPa ⁻¹ (<3 kPa)	−3–6 kPa	36
Capacitive	air gap	0.0018 nF/kPa	−0.8–0.8 kPa	38
Capacitive	ion gel	25.61 nF/kPa (0–100 kPa), 84.45 nF/kPa (0 ~ −70 kPa)	−98–100 kPa	our work

trend of capacitance change with air pressure can be measured while observing using a portable microscope. In order to get a clear view of the microstructure under air pressure, a rougher no. 100# sandpaper was chosen as the template. As shown in Figure 3c, the change of contact area at one contact site was observed under different air pressures, and the capacitance was recorded. The microscopic observation video is shown in the Video S1. The contact area of this site at standard atmospheric pressure was used as a reference. To obtain the normalized area at each air pressure, the areas at other air pressures are divided by the reference value. In Figure 3b, the normalized contact area is proportional to the magnitude of the air pressure and proportional to the capacitance value. It visually verifies the working principle of the sensor.

2.4. Performance of the Flexible Sensor. The sensitivity of the sensor is calculated by the equation

$$S = \delta(\Delta C)/\delta P \quad (1)$$

where ΔC is the relative change in capacitance ($C - C_0$) and P is the relative atmospheric pressure. Due to the specific nature of the negative pressure that the sensor needs to detect, the initial capacitance needs to be large, so following the traditional formula does not reflect the true performance. By plotting the tangent of the P – ΔC curve, we are able to calculate the sensitivity of the sensor in nF/kPa, which is the same as these reports using nF/kPa as the unit of sensitivity.^{41,43,44} As shown in Figure 4a, a sensor has high

sensitivity. The negative pressure sensitivity is up to 84.45 nF/kPa, while the positive pressure sensitivity is 25.61 nF/kPa. Our sensor also has a greater range of positive and negative pressure tests than previously reported, as shown in Table 1.

As shown in Figure 4b, the sensor has a positive pressure detection limit of approximately 1 kPa and a negative pressure detection limit of approximately 0.1 kPa, which can be estimated by gradually reducing the range of air pressure changes. In order to investigate the response time, we used a 100 mL syringe for the test (Figure S5 for test schematic, Supporting Information). The sensor was attached to the bottom of the syringe piston and the lead was threaded through the needle port to connect to the LCR tester. The piston was pushed to an initial position of 40 mL, and then the needle port was plugged. In Figure 4e, the syringe piston was quickly pushed to 20 mL and then immediately released. According to the formula

$$P_1 V_1 = P_2 V_2 \quad (2)$$

the relative air pressure is calculated to be 101 kPa at 20 mL volume. Its response time is 250 ms, and the recovery time (about 420 ms) is longer because of the hysteresis when it is withdrawn. Similarly, when testing the negative pressure, the piston was quickly pulled to 60 mL and then released. At this time, the relative air pressure was calculated to be −33.67 kPa, and the response times are 250 and 340 ms. But the syringe applies instantaneous positive or negative pressure, the process itself takes a certain amount of time. Thus, the actual response

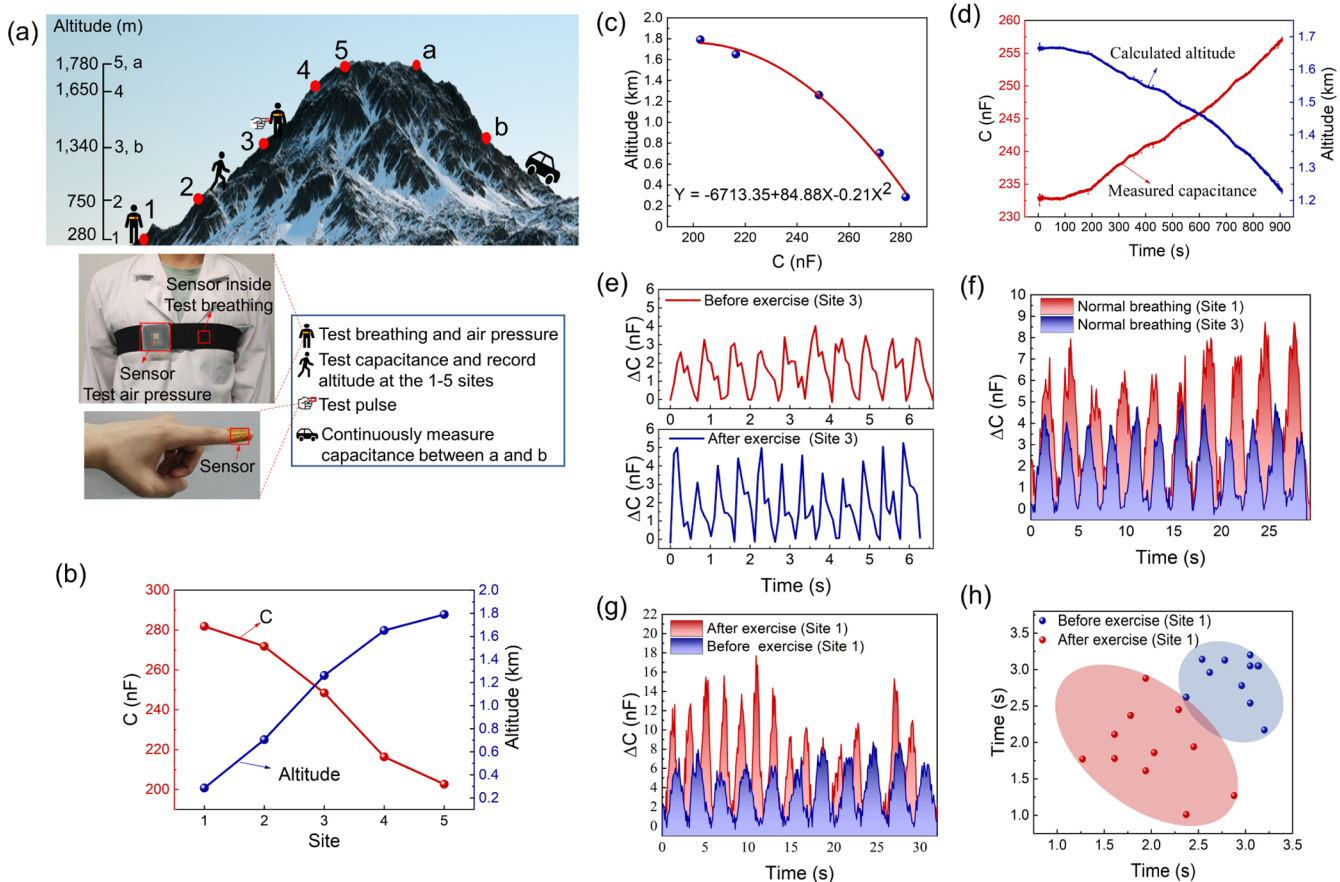


Figure 5. Application of the flexible sensor in wearable monitoring. (a) Schematic diagram of the test process during the ascent and descent, and wear methods of sensors on one's body to test breathing and pulse rates. (b) Capacitance of the sensor and the corresponding altitude measured at the five red points during the ascent. (c) Quadratic term function is fitted according to the correspondence between the capacitance and altitude. (d) Continuous capacitance measured by driving down between points a and b, which is brought into the fitted function to get the corresponding altitude. (e) Effect of exercise on pulse: the pulse frequency becomes faster and the peak of capacitance is higher after exercise. (f) Effect of altitude on breathing: high altitude makes one's breathing short. (g) Effect of exercise on breathing: exercise makes breathing deeper and faster, the peak of device capacitance indicates the depth of breathing and the number of peaks indicates the frequency. (h) Cloud plot of breathing points before and after exercise. The horizontal coordinate is the duration of one breath, and the vertical coordinate is the duration of the next breath.

time should be shorter. Moreover, we also used weights for routine response time and detection limit tests (Figures S6 and S7, Supporting Information). The compressive strain–stress curve of the sensor is shown in Figure S8 (Supporting Information). We can see better performance of our sensors in detecting positive pressure responses such as physiological signals as well. Figure 4d,e shows the cycling tests at relative air pressures of 20 and -20 kPa for the evaluation of cycling stability. Due to the specific nature of the device requiring manual testing, unlike other reported cycles, only 100 positive and negative pressure cycles were tested. Figure 4f shows the capacitance variation of the sensor in flat and different bending curvature states. The different bending curvatures were achieved by affixing the sensor to beakers of different capacities (Figure S5, Supporting Information). 100 mL/50 mL/25 mL beakers have a radius of 2.64 cm/2.32 cm/1.91 cm, respectively. It is noting that the sensor maintains the ability of detecting both positive and negative pressures, although the bending increases the initial capacitance, resulting in a decrease in pressure sensitivity.

2.5. Applications. Our sensors could be wearable to detect physiological signals and altitude changes, based on changes in their have capacitance. The test procedure is shown in Figure 5a. The sensor was attached to the inside of the tie near the

body for the breathing test, and the sensor was attached to the bottom of a small box and secured to the outside of the tie for the barometric pressure test. To test pulse, the sensor was wrapped around the fingertips with tape. The capacitance value of the sensor was tested at five positions when going up a hill. On the way down the hill, the continuous capacitance change was tested between points a and b. In Figure 5b, the capacitance decreased gradually as the altitude rose during the ascent. Figure 5c shows a function fitted from the capacitance versus altitude during the ascent. By plugging the continuous capacitance measured on the downhill into the function, the corresponding altitude change is obtained in Figure 5d. It is worth noting that there are obvious gentle sections (0–100 s, 400–450 s, etc.) in the calculated altitude curve, which results from stops or gentler slopes during the downhill drive. For positive pressure applications, this flexible pressure sensor could detect the rate of breathing, pulse beat, and so forth. Figure 5e shows that the sensor can measure at least two peaks of the pulse. And the pulse at rest and after exercise are tested separately to investigate the effect of exercise on the pulse. Clearly, the post-exercise pulse beats faster and has a larger peak than the pre-exercise pulse. Figure 5f compares normal breathing at site 1 and site 3 and shows that a high altitude makes a person short of breath. The effects of exercise on

breathing are shown in Figure 5g. After exercise, one needs more oxygen and therefore breathes faster and deeper, which can be corresponded to the change in capacitance. Meanwhile, it can be seen from the point cloud plot in Figure 5h that the distribution area of point cloud becomes larger after exercise, reflecting the heart rate malfunction.⁴⁵ Our sensor can detect not only the rise and fall of the chest during breathing but also the nasal breath, which can likewise reflect the frequency and depth of breathing (Figure S9, Supporting Information).

3. CONCLUSIONS

In summary, we reported a flexible large-range high-sensitive capacitive pressure sensor based on ionic gel, which was capable of measuring both positive and negative pressures. The microstructure was introduced to the surface of IG, and the sensor was encapsulated by vacuum laminator to form a confined environment. The contact state between IG and electrodes was changed under pressure, enabling the detection of both positive and negative pressures. And the preparation is simple and low-cost. The sensor exhibits a large detection range (-98 to 100 kPa) and high sensitivity ($S = 84.45$ nF/kPa for the -70 to 0 kPa region, $S = 25.61$ nF/kPa for the 0 – 100 kPa region). The sensor also exhibits good flexibility and cycling stability and could meet the requirements of wearable application. Furthermore, the wearable monitoring of atmospheric pressure, pulse, and breath on the way up and down the hill have been demonstrated, showing that the full-pressure sensor based on ionic gel have a wider range of applications in wearable electronics.

4. EXPERIMENTAL SECTION

4.1. Preparation of Microstructured IG Dielectric Layers. PVA ($M_w = 44.05$, purchased from Aladdin Industrial Corporation) of 9 g was added to a beaker containing 81 mL of heated deionized water in a ratio of $1:9$. The solution was then dissolved by mechanical stirring at 100 °C for 1 h. It was then cooled to room temperature and phosphoric acid solution with a mass fraction of 0.69 g/mL was added. The IG liquid was obtained by putting in a magnet and stirring with vibration at room temperature for 2 h. Next, we stuck the required sandpaper on a flat iron plate and fixed the customized mold on the sandpaper. The scanning electron microscopy (SEM) image of sandpaper is shown in Figure S10 (Support Information). We then poured in an appropriate amount of IG liquid and placed it in a drying oven at 40 ° for 12 h. It may take longer depending on the ambient humidity, and so forth. After curing, the IG film was removed.

4.2. Preparation of Electrodes and Sensors. First, the silver paste was printed onto the PET substrate by patterning the stencil and then baking it at 90 ° for 20 min. Next, the OCA is cut into a 2×2 cm² size with a laser cutter and a 1.1×1.1 cm² square hole is cut in the middle. The OCA is attached to one side of the electrode substrate to expose the electrode area. After that, the IG film is cut to a 1×1 cm² size and placed into the exposed conductive area, and the top electrode is gently covered. A face-to-face sandwich structure is formed, leaving a gap at this point. Finally, the sensor to be encapsulated is placed in a vacuum laminator for laminating and encapsulating with a pressure of about 4 bar.

4.3. Loading Positive and Negative Pressure. The test equipment is customized using a metal chamber with an outer diameter of 18 cm, an inner diameter of 15 cm, and an overall height of about 20 cm. A metal chamber is externally connected to an oil-free air compressor (model OTS-550) to provide a positive pressure environment. An external vacuum pump is connected to provide a negative pressure environment, with high power to achieve maximum negative pressure.

4.4. Characterization. The microstructure of PVA/H₃PO₄ films was characterized by a scanning electron microscope (JSM-7800F,

JEOL, Tokyo, Japan). The contact area variation at different air pressures was characterized by a WiFi CNC metal head microscope purchased online. The capacitance was measured using an LCR tester (2827A, TONGHUI) with a voltage setting of 30 mV and a frequency of 1 kHz. All the demonstrations for wearable detection, including breathing, pulse, and air pressure, were conducted by the leading author with informed consent.

■ ASSOCIATED CONTENT

SI Supporting Information

The Supporting Information is available free of charge at <https://pubs.acs.org/doi/10.1021/acsami.3c00916>.

Schematic diagram of large-area preparation of Ag electrode by the screen printing process; sensitivities of IG films with different thicknesses are compared under negative pressure; performance pattern of sensors prepared with different contents of phosphoric acid; performance pattern of sensors prepared with different water contents; photograph of the sensor attached to the beaker cup and photograph of the sensor in a syringe; weight of 50 g placed on the sensor to test the response time; sensor detect a minimum weight of 500 mg; and sensor detecting nasal breath and reflecting the frequency and depth of breathing and diagram of the test method ([PDF](#))

Video of microscopic observation ([MP4](#))

■ AUTHOR INFORMATION

Corresponding Author

Dapeng Wei – State Key Laboratory of Trauma, Burn and Combined Injury, Third Military Medical University, Chongqing 400042, China; Chongqing Institute of Green and Intelligent Technology, Chinese Academy of Sciences, Chongqing 400714, China; Chongqing School, University of Chinese Academy of Sciences, Chongqing 400714, China; Chongqing Institute of Graphene, Chongqing 400714, China; orcid.org/0000-0002-3575-617X; Email: dpwei@cigit.ac.cn

Authors

Mengqin Zhang – Chongqing Institute of Green and Intelligent Technology, Chinese Academy of Sciences, Chongqing 400714, China; Chongqing University of Technology, Chongqing 400054, China; Chongqing School, University of Chinese Academy of Sciences, Chongqing 400714, China

Mingxin Gu – Chongqing Institute of Green and Intelligent Technology, Chinese Academy of Sciences, Chongqing 400714, China; Chongqing School, University of Chinese Academy of Sciences, Chongqing 400714, China

Li Shao – Chongqing Institute of Green and Intelligent Technology, Chinese Academy of Sciences, Chongqing 400714, China; Chongqing School, University of Chinese Academy of Sciences, Chongqing 400714, China

Guanyin Cheng – Chongqing Institute of Green and Intelligent Technology, Chinese Academy of Sciences, Chongqing 400714, China; Chongqing University of Technology, Chongqing 400054, China; Chongqing School, University of Chinese Academy of Sciences, Chongqing 400714, China

Hailin Gao – Chongqing Institute of Green and Intelligent Technology, Chinese Academy of Sciences, Chongqing

400714, China; Chongqing School, University of Chinese Academy of Sciences, Chongqing 400714, China
Bihao Sun — Chongqing Institute of Green and Intelligent Technology, Chinese Academy of Sciences, Chongqing 400714, China; Chongqing School, University of Chinese Academy of Sciences, Chongqing 400714, China
Sen Li — State Key Laboratory of Trauma, Burn and Combined Injury, Third Military Medical University, Chongqing 400042, China
Tian Tang — Chongqing Institute of Green and Intelligent Technology, Chinese Academy of Sciences, Chongqing 400714, China
Nan Li — Chongqing Institute of Graphene, Chongqing 400714, China
Yuanbang Yi — Chongqing Institute of Graphene, Chongqing 400714, China
Dacheng Wei — Chongqing School, University of Chinese Academy of Sciences, Chongqing 400714, China;
orcid.org/0000-0003-3593-9897
Ce Yang — State Key Laboratory of Trauma, Burn and Combined Injury, Third Military Medical University, Chongqing 400042, China

Complete contact information is available at:
<https://pubs.acs.org/10.1021/acsami.3c00916>

Author Contributions

The manuscript was written through contributions of all authors. All authors have given approval to the final version of the manuscript.

Notes

The authors declare no competing financial interest.

ACKNOWLEDGMENTS

This work was supported by the Open Project of the State Key Laboratory of Trauma, Burn and Combined Injury, Third Military Medical University (NO.SKL202102), Chongqing Talents Program (CQYC2020030146), Project of Chongqing Science and Technology Bureau (cstc2021ycjh-bgzxm0345), Key R&D and Transformation of Science and Technology Projects in the Tibet Autonomous Region (XZ2022RH001), Chongqing Bayu Scholar Program (DP2020036), and Chongqing Entrepreneurship and Innovation Support Program for Overseas Students Returning to China.

REFERENCES

- (1) Schwartz, G.; Tee, B. C. K.; Mei, J.; Appleton, A. L.; Kim, D. H.; Wang, H.; Bao, Z. Flexible Polymer Transistors with High Pressure Sensitivity for Application in Electronic Skin and Health Monitoring. *Nat. Commun.* **2013**, *4*, 1859.
- (2) Boutry, C. M.; Nguyen, A.; Lawal, Q. O.; Chortos, A.; Rondeau-Gagné, S. R.; Bao, Z. A Sensitive and Biodegradable Pressure Sensor Array for Cardiovascular Monitoring. *Adv. Mater.* **2015**, *27*, 6954.
- (3) Kim, J.; Chou, E.-F.; Le, J.; Wong, S.; Chu, M.; Khine, M. Soft Wearable Pressure Sensors for Beat-to-Beat Blood Pressure Monitoring. *Adv. Healthcare Mater.* **2019**, *8*, 1900109.
- (4) Sundaram, S.; Kellnhofer, P.; Li, Y.; Zhu, J.; Torralba, A.; Matusik, W. Learning the Signatures of the Human Grasp Using A Scalable Tactile Glove. *Nat* **2019**, *569*, 698.
- (5) Fan, W.; He, Q.; Meng, K.; Tan, X.; Zhou, Z.; Zhang, G.; Yang, J.; Wang, Z. Machine-Knitted Washable Sensor Array Textile for Precise Epidermal Physiological Signal Monitoring. *Sci. Adv.* **2020**, *6*, No. eaay2840.
- (6) Guo, Y.; Guo, Z.; Zhong, M.; Wan, P.; Zhang, W.; Zhang, L. A flexible Wearable Pressure Sensor with Bioinspired Microcrack and

Interlocking for Full-Range Human–Machine Interfacing. *Small* **2018**, *14*, 1803018.

- (7) Yu, Y.; Nassar, J.; Xu, C.; Min, J.; Yang, Y.; Dai, A.; Doshi, R.; Huang, A.; Song, Y.; Gehlhar, R.; Ames, A.; Gao, W. Biofuel-Powered Soft Electronic Skin with Multiplexed and Wireless Sensing for Human-Machine Interfaces. *Sci. Robot.* **2020**, *5*, No. eaaz7946.
- (8) Ruth, S. R. A.; Feig, V. R.; Tran, H.; Bao, Z. Microengineering Pressure Sensor Active Layers for Improved Performance. *Adv. Funct. Mater.* **2020**, *30*, 2003491.
- (9) Pan, L.; Chortos, A.; Yu, G.; Wang, Y.; Isaacson, S.; Allen, R.; Shi, Y.; Dauskardt, R.; Bao, Z. An Ultra-Sensitive Resistive Pressure Sensor Based on Hollow-Sphere Microstructure Induced Elasticity in Conducting Polymer Film. *Nat. Commun.* **2014**, *5*, 3002.
- (10) Lou, Z.; Chen, S.; Wang, L.; Jiang, K.; Shen, G. An Ultra-Sensitive and Rapid Response Speed Graphene Pressure Sensors for Electronic Skin and Health Monitoring. *Nano Energy* **2016**, *23*, 7.
- (11) Yu, J.; Hou, X.; He, J.; Cui, M.; Wang, C.; Geng, W.; Mu, J.; Han, B.; Chou, X. Ultra-Flexible and High-Sensitive Triboelectric Nanogenerator as Electronic Skin for Self-Powered Human Physiological Signal Monitoring. *Nano Energy* **2020**, *69*, 104437.
- (12) Boutry, C. M.; Negre, M.; Jorda, M.; Vardoulis, O.; Chortos, A.; Khatib, O.; Bao, Z. A Hierarchically Patterned, Bioinspired E-Skin Able to Detect the Direction of Applied Pressure for Robotics. *Sci. Robot.* **2018**, *3*, No. eaau6914.
- (13) Shi, R.; Lou, Z.; Chen, S.; Shen, G. Flexible and Transparent Capacitive Pressure Sensor with Patterned Microstructured Composite Rubber Dielectric for Wearable Touch Keyboard Application. *Sci. China Mater.* **2018**, *61*, 1587.
- (14) Mishra, R. B.; El-Atab, N. E.; Hussain, A. M.; Hussain, M. M. Recent Progress on Flexible Capacitive Pressure Sensors: from Design and Materials to Applications. *Adv. Mater. Technol.* **2021**, *6*, 2001023.
- (15) Ruth, S. R. A.; Beker, L.; Tran, H.; Feig, V. R.; Matsuhsisa, N.; Bao, Z. Rational Design of Capacitive Pressure Sensors Based on Pyramidal Microstructures for Specialized Monitoring of Biosignals. *Adv. Funct. Mater.* **2020**, *30*, 1903100.
- (16) Yang, J. C.; Kim, J. O.; Oh, J.; Kwon, S. Y.; Sim, J. Y.; Kim, D. W.; Choi, H. B.; Park, S. Microstructured Porous Pyramid-Based Ultrahigh Sensitive Pressure Sensor Insensitive to Strain and Temperature. *ACS Appl. Mater. Interfaces* **2019**, *11*, 19472.
- (17) Li, T.; Luo, H.; Qin, L.; Wang, X.; Xiong, Z.; Ding, H.; Gu, Y.; Liu, Z.; Zhang, T. Flexible Capacitive Tactile Sensor Based on Micropatterned Dielectric Layer. *Small* **2016**, *12*, 5042.
- (18) Xiong, Y.; Shen, Y.; Tian, L.; Hu, Y.; Zhu, P.; Sun, R.; Wong, C. P. A Flexible, Ultra-Highly Sensitive and Stable Capacitive Pressure Sensor with Convex Microarrays for Motion and Health Monitoring. *Nano Energy* **2020**, *70*, 104436.
- (19) Yang, J.; Luo, S.; Zhou, X.; Li, J.; Fu, J.; Yang, W.; Wei, D. Flexible, Tunable and Ultrasensitive Capacitive Pressure Sensor with Micro-Conformal Graphene Electrodes. *ACS Appl. Mater. Interfaces* **2019**, *11*, 14997.
- (20) Luo, Z.; Chen, J.; Zhu, Z.; Li, L.; Su, Y.; Tang, W.; Omisore, O. M.; Wang, L.; Li, H. High-Resolution and High-Sensitivity Flexible Capacitive Pressure Sensors Enhanced by a Transferable Electrode Array and a Micropillar–PVDF Film. *ACS Appl. Mater. Interfaces* **2021**, *13*, 7635.
- (21) Qiu, Z.; Wan, Y.; Zhou, W.; Yang, J.; Yang, J.; Huang, J.; Zhang, J.; Liu, Q.; Huang, S.; Bai, N.; Wu, Z.; Hong, W.; Wang, H.; Guo, C. F. Ionic Skin with Biomimetic Dielectric Layer Templated from Calathea Zebrina Leaf. *Adv. Funct. Mater.* **2018**, *28*, 1802343.
- (22) Li, R.; Zhou, Q.; Bi, Y.; Cao, S.; Xia, X.; Yang, A.; Li, S.; Xiao, X. Research Progress of Flexible Capacitive Pressure Sensor for Sensitivity Enhancement Approaches. *Sens. Actuators, A* **2021**, *321*, 112425.
- (23) Senokos, E.; Reguero, V.; Cabana, L.; Palma, J.; Marcilla, R.; Vilatela, J. J. Large-Area, All-Solid, and Flexible Electric Double Layer Capacitors Based on CNT Fiber Electrodes and Polymer Electrolytes. *Adv. Mater. Technol.* **2017**, *2*, 1600290.

- (24) She, Z.; Ghosh, D.; Pope, M. A. Decorating Graphene Oxide with Ionic Liquid Nanodroplets: an Approach Leading to Energy-Dense, High-Voltage Supercapacitors. *ACS Nano* **2017**, *11*, 10077.
- (25) Song, Z.; Duan, H.; Miao, L.; Ruhlmann, L.; Lv, Y.; Xiong, W.; Zhu, D.; Li, L.; Gan, L.; Liu, M. Carbon Hydrangeas with Typical Ionic Liquid Matched Pores for Advanced Supercapacitors. *Carbon* **2020**, *168*, 499.
- (26) Kim, I.; Kim, B. S.; Nam, S.; Lee, H. J.; Chung, H. K.; Cho, S. M.; Luu, T. H. T.; Hyun, S.; Kang, C. Cross-Linked Poly (Vinylidene Fluoride-Cohexafluoropropene) (PVDF-co-HFP) Gel Polymer Electrolyte for Flexible Li-Ion Battery Integrated with Organic Light Emitting Diode (OLED). *Mater* **2018**, *11*, 543.
- (27) Niu, H.; Wang, L.; Guan, P.; Zhang, N.; Yan, C.; Ding, M.; Guo, X.; Huang, T.; Hu, X. Recent Advances in Application of Ionic Liquids in Electrolyte of Lithium Ion Batteries. *J. Energy Storage* **2021**, *40*, 102659.
- (28) Lieb, J.; Demontis, V.; Prete, D.; Ercolani, D.; Zannier, V.; Sorba, L.; Ono, S.; Beltram, F.; Sacépé, B.; Rossella, F. Ionic-Liquid Gating of InAs Nanowire-Based Field-Effect Transistors. *Adv. Funct. Mater.* **2019**, *29*, 1804378.
- (29) Soeda, J.; Matsui, H.; Okamoto, T.; Osaka, I.; Takimiya, K.; Takeya, J. Highly Oriented Polymer Semiconductor Films Compressed at the Surface of Ionic Liquids for High-Performance Polymeric Organic Field-Effect Transistors. *Adv. Mater.* **2014**, *26*, 6430.
- (30) Kim, J. S.; Lee, S. C.; Hwang, J.; Lee, E.; Cho, K.; Kim, S. J.; Kim, D. H.; Lee, W. H. Enhanced Sensitivity of Iontronic Graphene Tactile Sensors Facilitated by Spreading of Ionic Liquid Pinned on Graphene Grid. *Adv. Funct. Mater.* **2020**, *30*, 1908993.
- (31) Cho, S. H.; Lee, S. W.; Yu, S.; Kim, H.; Chang, S.; Kang, D.; Hwang, I.; Kang, H. S.; Jeong, B.; Kim, E. H.; Cho, S. M.; Kim, K. L.; Lee, H.; Shim, W.; Park, C. Micropatterned Pyramidal Ionic Gels for Sensing Broad-Range Pressures with High Sensitivity. *ACS Appl. Mater. Interfaces* **2017**, *9*, 10128.
- (32) Chhetry, A.; Kim, J.; Yoon, H.; Park, J. Y. Ultrasensitive Interfacial Capacitive Pressure Sensor Based on a Randomly Distributed Microstructured Iontronic Film for Wearable Applications. *ACS Appl. Mater. Interfaces* **2018**, *11*, 3438.
- (33) Bai, N.; Wang, L.; Wang, Q.; Deng, J.; Wang, Y.; Lu, P.; Huang, J.; Li, G.; Zhang, Y.; Yang, J.; Xie, K.; Zhao, X.; Guo, C. F. Graded Intrafillable Architecture-Based Iontronic Pressure Sensor with Ultra-Broad-Range High Sensitivity. *Nat. Commun.* **2020**, *11*, 209.
- (34) Kier, W. M.; Smith, A. M. The Structure and Adhesive Mechanism of Octopus Suckers. *Integr. Comp. Biol.* **2002**, *42*, 1146.
- (35) Xiong, W.; Zhu, C.; Guo, D.; Hou, C.; Yang, Z.; Xu, Z.; Qiu, L.; Yang, H.; Li, K.; Huang, Y. Bio-Inspired, Intelligent Flexible Sensing Skin for Multifunctional Flying Perception. *Nano Energy* **2021**, *90*, 106550.
- (36) Xiong, W.; Guo, D.; Yang, Z.; Zhu, C.; Huang, Y. Conformable, Programmable and Step-Linear Sensor Array for Large-Range Wind Pressure Measurement on Curved Surface. *Sci. China Mater.* **2020**, *63*, 2073.
- (37) Shi, H.; Al-Rubaiai, M.; Holbrook, C. M.; Miao, J.; Pinto, T.; Wang, C.; Tan, X. Screen-Printed Soft Capacitive Sensors for Spatial Mapping of both Positive and Negative Pressures. *Adv. Funct. Mater.* **2019**, *29*, 1809116.
- (38) An, L.; Lu, T.; Xu, J.; Wang, Z.; Xu, M.; Wang, T. Soft Sensor for Measuring Wind Pressure. *Int. J. Mech. Sci.* **2018**, *141*, 386.
- (39) Sun, J. Y.; Keplinger, C.; Whitesides, G. M.; Suo, Z. Ionic Skin. *Adv. Mater.* **2014**, *26*, 7608.
- (40) Keplinger, C.; Sun, J. Y.; Foo, C. C.; Rothemund, P.; Whitesides, G. M.; Suo, Z. Stretchable, Transparent, Ionic Conductors. *Science* **2013**, *341*, 984.
- (41) Nie, B.; Li, R.; Cao, J.; Brandt, J. D.; Pan, T. Flexible Transparent Iontronic Film for Interfacial Capacitive Pressure Sensing. *Adv. Mater.* **2015**, *27*, 6055.
- (42) Oldham, K. B. A Gouy–Chapman–Stern Model of the Double Layer at a (Metal)/(Ionic Liquid) Interface. *J. Electroanal. Chem.* **2008**, *613*, 131.
- (43) Li, S.; Pan, N.; Zhu, Z.; Li, R.; Li, B.; Chu, J.; Li, G.; Chang, Y.; Pan, T. All-in-One Iontronic Sensing Paper. *Adv. Funct. Mater.* **2019**, *29*, 1807343.
- (44) Keum, K.; Eom, J.; Lee, J. H.; Heo, J. S.; Park, S. K.; Kim, Y. H. Fully-Integrated Wearable Pressure Sensor Array Enabled by Highly Sensitive Textile-Based Capacitive Ionotronic Devices. *Nano Energy* **2021**, *79*, 105479.
- (45) Guzik, P.; Piskorski, J.; Krauze, T.; Schneider, R.; Wesseling, K. H.; Wykretowicz, A.; Wysocki, H. Correlations between the Poincaré Plot and Conventional Heart Rate Variability Parameters Assessed during Paced Breathing. *J. Physiol. Sci.* **2007**, *57*, 63.



CAS BIOFINDER DISCOVERY PLATFORM™

STOP DIGGING THROUGH DATA — START MAKING DISCOVERIES

CAS BioFinder helps you find the right biological insights in seconds

Start your search

